UinTSeg: Unified Infant Brain Tissue Segmentation with Anatomy Delineation

Jiameng Liu[1,⋆], Feihong Liu[2,1,⋆], Kaicong Sun[1], Yuhang Sun[1], Jiawei Huang[1], Caiwen Jiang[1], Islem Rekik[5], and Dinggang Shen[1,3,4] ✉

[1] School of Biomedical Engineering & State Key Laboratory of Advanced Medical Materials and Devices, ShanghaiTech University, Shanghai, China
Dinggang.Shen@gmail.com
[2] School of Information Science and Technology, Northwest University, Xi'an, China
[3] Shanghai United Imaging Intelligence Co., Ltd., Shanghai, China
[4] Shanghai Clinical Research and Trial Center, Shanghai, China,
[5] BASIRA Lab, Imperial-X (I-X) and Department of Computing, Imperial College London, London, UK

Abstract. Accurate brain tissue segmentation is a vital prerequisite for charting infant brain development and for diagnosing early brain disorders. However, due to inherently ongoing myelination and maturation, the intensity distributions of gray matter (GM) and white matter (WM) on T1-weighted (T1w) data undergo substantial *variations in intensity* from neonatal to 24 months. Especially at the ages around 6 months, the intensity distributions of GM and WM are highly overlapped. These physiological phenomena pose great challenges for automatic infant brain tissue segmentation, even for expert radiologists. To address these issues, in this study, we present a unified infant brain tissue segmentation (*UinTSeg*) framework to accurately segment brain tissues of infants aged 0-24 months using a single model. *UinTSeg* comprises two stages: 1) boundary extraction and 2) tissue segmentation. In the first stage, to alleviate the difficulty of tissue segmentation caused by variations in intensity, we extract the *intensity-invariant* tissue boundaries from T1w data driven by edge maps extracted from the Sobel filter. In the second stage, the *Sobel edge maps* and *extracted boundaries* of GM, WM, and cerebrospinal fluid (CSF) are utilized as *intensity-invariant* anatomy information to ensure unified and accurate tissue segmentation in infants age period of 0-24 months. Both stages are built upon an attention-based surrounding-aware segmentation network (*ASNet*), which exploits the contextual information from multi-scale patches to improve the segmentation performance. Extensive experiments on the baby connectome project dataset demonstrate the superiority of our proposed framework over five state-of-the-art methods.

Keywords: Infant brain tissue segmentation · Boundary delineation · Multi-scale segmentation.

⋆ These authors contributed equally to this work.

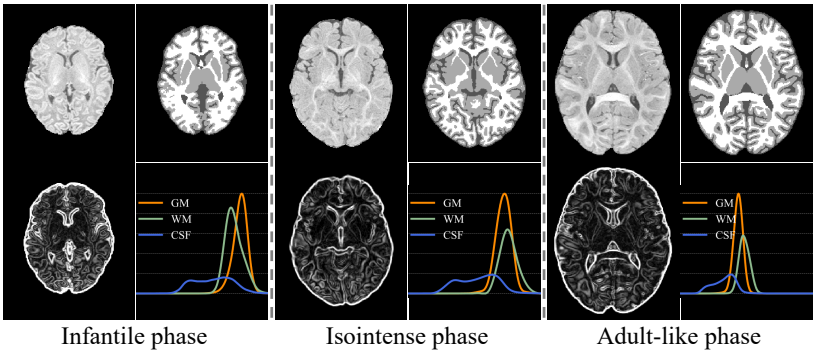

Fig. 1. Varying tissue intensity distributions along ongoing brain development.

1 Introduction

Infant brain grows rapidly during its first two years of life, underlying synaptogenesis and myelination after the stabilization of brain anatomy [24,6,8,21]. Accurate segmentation of brain tissues (*i.e.*, GM, WM, and CSF) from structural MRI (sMRI) data enables reliable charting of this ongoing and dramatic development period, which sheds light on understanding early learning and pathological mechanisms [14,27,16,28,13,12]. Challenges, due to the ongoing and dramatic myelination and maturation processes, manifest in GM and WM *variations in intensity* from sMRI data, which hinders accurate brain tissue segmentation of infants, although brain anatomy has been stabilized already. As depicted in Fig. 1, the rapid brain development is demonstrated by the varying tissue intensity distributions of three roughly-divided phases [3], *i.e.*, 1) the infantile phase ($\leq$5 months), 2) the isointense phase (6$-$9 months), and 3) the adult-like phase (10$-$24 months).

The *variations in intensity* incur severe challenges for both categories of segmentation methods: 1) registration-based and 2) learning-based, in the literatures. Registration-based methods typically warp tissue maps from a predefined brain atlas to individual subjects [20,25,29,11], indirectly obtaining the segmented tissues. However, accurate registration could hardly be guaranteed due to substantial variations in size and in intensity contrast between GM and WM of the infant brain data (0-24 months). This challenge is particularly pronounced for segmenting sMRI data in the isointense phase, where registration struggles with unclear tissue boundaries, leading to notable registration and segmentation errors. By contrast, recent advances in learning-based algorithms improve the segmentation accuracy by individualizing infant brain tissue segmentation [26,17,1,27,22]. They have to train a range of age-specific models to segment infant brain tissues at each age period [27]. Also, targeting to improve the segmentation accuracy in the isointense phase, there are specific efforts in segmenting isointense phase infant brain tissue by utilizing adult-like phase data

with clearer tissue boundaries [2,14]. However, these methods are predominantly tailored for the age periods, and it has to segment brain tissues across 0-24 months with a list of different models. Considering the individual heterogeneity, those isolated models may lose fidelity and cause longitudinal inconsistency in segmenting the tissues.

In this study, to address the aforementioned challenges, we propose a unified infant brain tissue segmentation framework, *UinTSeg*, to achieve longitudinally consistent and accurate tissue segmentation for infants aged from neonatal to 24 months in an integrated framework. Our proposed *UinTSeg* consists of two stages: 1) boundary extraction and 2) tissue segmentation, as depicted in Fig. 2. In the first stage, a boundary extraction network utilizes the coarse edge maps of tissues obtained by Sobel filter [10] to extract *intensity-invariant* boundaries of GM, WM, and CSF, respectively, in delineating brain anatomy. In the second stage, both *Sobel edge maps* and *extracted boundaries* serve as *intensity-invariant* anatomy information to mitigate *variations in intensity* in infants age period of 0-24 months. Considering the most difficult case, isointense phase data, *UinTSeg* additionally capitalizes a synthesis model from our previous work [14] to transform isointense phase T1w data, characterized by unclear tissue contrast, into an adult-like phase T1w data with clearer tissue edges before extracting *Sobel edge maps*. It is worth noting that the networks in both stages are built upon an attention-based surrounding-aware segmentation network (*ASNet*) to leverage comprehensive contextual information, which is proven effective in enhancing segmentation performance. More specifically, *ASNet* simultaneously segment two scales of patches, namely local patches with a regular receptive field and surrounding patches with a larger receptive field. Features extracted from the surrounding patches, rich in contextual information, are integrated into the local patch segmentation branch using an attention-based cross-branch fusion (CBF) module to enhance tissue segmentation performance. Extensive experiments are conducted on the baby connectome project (BCP) [7] dataset, and the results demonstrate the superiority of our proposed *UinTSeg* framework.

2 Method

Our proposed *UinTSeg* framework comprises two stages: 1) boundary extraction and 2) tissue segmentation (Sec. 2.1). The networks employed in both stages share the same network architecture, *ASNet*, without sharing the weights. *ASNet* is elaborately devised to exploit abundant contextual information from multi-scale patches (Sec. 2.2). In Sec. 2.3, we introduce the implementation details of *UinTSeg*.

2.1 Anatomy-guided Tissue Segmentation

In the two stages, *UinTSeg* first delineates tissue boundaries and then capitalizes the extracted boundaries to resolve the segmentation challenge of *variations in intensity*. In the first stage, as shown in Fig. 2 (a), *UinTSeg* employs

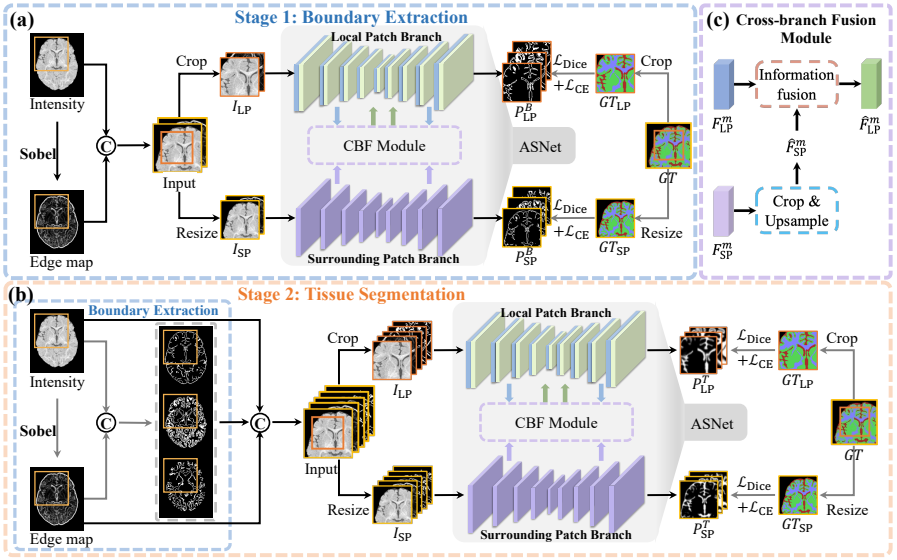

Fig. 2. Illustration of our proposed unified infant brain tissue segmentation (*UinTSeg*) framework, with (a) Boundary extraction, (b) Tissue segmentation, and (c) Cross-branch fusion (CBF) modules. (Boundaries extracted from GT_{LP} and GT_{SP} are omitted for simplicity)

the Sobel filter [10] to obtain edge maps from T1w data. The *Sobel edge maps*, serving as coarse *intensity-invariant* anatomical information, are concatenated with the corresponding T1w data as the input of the boundary extraction network in stage 1 to guide the boundary extraction network to accurately extract tissue boundaries of GM, WM, and CSF in delineating more accurate *intensity-invariant* information of the brain anatomy. In the second stage, as shown in Fig. 2 (b), beyond *Sobel edge maps* and T1w data, boundaries extracted in stage 1 are concatenated additionally. Under the guidance of this extracted *intensity-invariant* anatomy information, the tissue segmentation network is tailored to segment GM, WM, and CSF, respectively.

UinTSeg, by this, mitigates the adverse effects of *variations in intensity* along the ongoing development period and tactically emphasizes tissue boundaries for the segmentation network. It is worth noting here again that the networks employed in both stages share the same network architecture in *ASNet* (detailed in Sec. 2.2), however, without sharing the weights.

2.2 Attention-based Surrounding-aware Segmentation Network

ASNet is designed as the core segmentation network in both boundary extraction and tissue segmentation stages. The input of *ASNet* in stage 1 is the concatenated T1w data and its corresponding *Sobel edge maps*; while in stage 2,

the extracted boundaries of GM, WM, and CSF are additionally concatenated. Besides the *intensity-invariant* anatomy information, *ASNet* enables extracting multi-scale features by employing two distinct scales of patches. As shown in Fig. 2, *ASNet* comprises two parallel segmentation branches, and each branch deals with a specific patch scale, *i.e.*, local patch (LP) and surrounding patch (SP). The input of *ASNet* is cropped into two-scale patches at the same center point location, denoted as local patch I_{LP} and surrounding path I_{SP}. The surrounding patch I_{SP} contains more contextual information within an enlarged region. These two patches are passed to the local patch branch and surrounding patch branch, respectively. Both branches are built on the 3D UNet [19] architecture, comprising the four-stage encoder and decoder with skip connections between the corresponding encoder and decoder layers.

Moreover, to integrate features from two segmentation branches in *ASNet*, we propose a cross-branch fusion (CBF) module, as shown in Fig. 2 (c) [4]. The CBF module first crops a central part of features F^m_{SP} from the surrounding patch branch at the m-th layer, based on the original size ratio between local and surrounding patches (orange and yellow box on Input in Fig. 2 (a) & (b)). The cropped features are then upsampled as $\hat{F}^m_{\text{SP}}$, which matches the size of features F^m_{LP} from the local patch branch at m-th layer. Then, the information fusion module (brown dashed box in Fig. 2 (c)), incorporated with both spatial- and channel-attention layers, is employed to fuse the features of the two branches layer-by-layer (denoted as $\hat{F}^m_{\text{LP}}$). By this, the CBF module merges the contextual features obtained from the surrounding patch branch with the local one, complementing the local patch features with a more comprehensive anatomy representation. During the training of the two stages, we utilize a hybrid loss functions, blending Dice loss $\mathcal{L}_{\text{Dice}}$ and cross-entropy loss $\mathcal{L}_{\text{CE}}$, which have been widely validated for medical image segmentation tasks [15].

2.3 Implementation Details

Our proposed *UinTSeg* is trained in two separate stages. We first train the edge extraction network, obtaining the tissue boundaries as input for the tissue segmentation network. The entire framework is implemented on PyTorch 1.7.1 and trained on a workstation equipped with an NVIDIA V100s GPU. We employ the Adam optimizer, and the initial learning rate is set as 0.001 with a 10% decay every 50 epochs. The patch sizes of the local and surrounding patches are set as $128 \times 128 \times 128$ and $160 \times 160 \times 160$, respectively. Our code and pre-trained model can be found in this link.

3 Experiments

3.1 Dataset and Evaluation Metrics

We collected T1w infant brain data from the BCP dataset [7] to train and evaluate our framework. This dataset comprises 672 T1w data scanned from 264 subjects, with an age range from 2 weeks to 24 months. All the data were acquired

Table 1. Quantitative comparison with 4 SOTA methods for ages 0-24 months.

Method	Dice (%) ↑			HD (*mm*) ↓			ASD×10 (*mm*) ↓		
	GM	WM	CSF	GM	WM	CSF	GM	WM	CSF
InfantFS	70.81±9.43	71.57±11.18	55.84±6.26	14.95±2.04	22.89±4.54	13.83±1.82	9.12±6.73	13.55±8.67	10.87±6.27
3D UNet	93.83±2.62	94.15±2.50	93.15±1.86	6.95±1.90	7.29±2.45	9.96±2.30	1.01±0.26	1.16±0.51	0.78±0.27
nnUNet	95.20±2.22	95.47±1.97	94.58±1.88	6.77±1.64	7.27±2.37	9.76±2.17	0.81±0.25	0.91±0.41	0.63±0.38
SwinUNetR	95.04±2.10	95.43±1.88	94.50±1.27	6.60±2.01	7.16±2.57	9.34±2.28	0.81±0.19	0.91±0.38	0.60±0.19
UinTSeg	**95.84±2.07**	**95.98±1.87**	**95.70±1.51**	**6.57±1.95**	**6.96±2.44**	**8.88±2.21**	**0.68±0.22**	**0.80±0.37**	**0.48±0.23**

Table 2. Quantitative comparison with 5 SOTA methods for the isointense phase.

Method	Dice (%) ↑			HD (*mm*) ↓			ASD×10 (*mm*) ↓		
	GM	WM	CSF	GM	WM	CSF	GM	WM	CSF
InfantFS	65.61±2.93	60.51±2.61	53.50±2.73	15.41±1.36	21.35±0.89	14.11±1.28	11.2±3.16	23.00±2.02	11.5±0.63
3D UNet	91.31±0.96	91.88±0.74	91.85±1.25	4.94±1.05	6.39±1.35	8.78±2.17	1.14±0.11	1.59±0.18	0.95±0.13
nnUNet	93.47±0.97	94.21±0.88	93.72±1.08	5.37±1.17	6.13±1.19	9.44±2.33	0.87±0.12	1.14±0.18	0.71±0.11
SwinUNetR	93.12±0.93	93.85±0.78	93.81±1.04	4.32±1.03	6.58±1.08	8.39±2.49	0.88±0.12	1.21±0.18	0.69±0.10
TMSN	94.33±1.01	95.11±0.86	**95.35±0.92**	6.08±1.26	6.54±1.04	**6.68±0.97**	0.73±0.13	1.03±0.19	**0.52±0.11**
UinTSeg	**94.66±0.64**	**95.24±0.56**	95.21±0.67	**4.31±0.54**	**6.01±1.03**	6.95±1.73	**0.69±0.08**	**0.94±0.12**	0.53±0.06

from diverse sites, using various scanners, and demographics, thereby enhancing the robustness of our *UinTSeg* framework. The ground-truth (GT) labels of GM, WM, and CSF were manually annotated by experienced radiologists. We first normalized the intensity of each T1w image to standard distribution using z-score normalization [18]. Notably, we only kept the top 99.99% of the intensity values of each image to mitigate the influence of outlier values. Then the data was randomly divided into three distinct subsets: *i*) 70% for training, *ii*) 10% for validation, and *iii*) 20% for testing. The data partitioning process is carried out independently for each subject to eliminate data leakage caused by the longitudinal scanning data of the same subject. The segmentation performance is comprehensively evaluated through three metrics: *i*) Dice score (Dice), *ii*) Hausdorff Distance (HD), and *iii*) Average Surface Distance (ASD) [23].

3.2 Comparison with SOTA Methods

To demonstrate the superiority of our proposed *UinTSeg*, we conducted a comprehensive comparison with five SOTA methods, including: 1) Infant FreeSurfer (InfantFS) [29], which utilizes a multi-atlas fusion strategy for infant tissue segmentation; 2) 3D UNet [19], a baseline single-scale segmentation network; 3) nnUNet [9], regarded as one of the most stable and general medical image segmentation methods; 4) SwinUNetR [5], an advanced Swin transformer-based segmentation network for 3D medical image segmentation; and 5) TMSN [14], an advanced learning-based isointense infant brain tissue segmentation network. To ensure a fair comparison, we utilized the same data splitting and training strategies as employed in *UinTSeg* for all the SOTA methods.

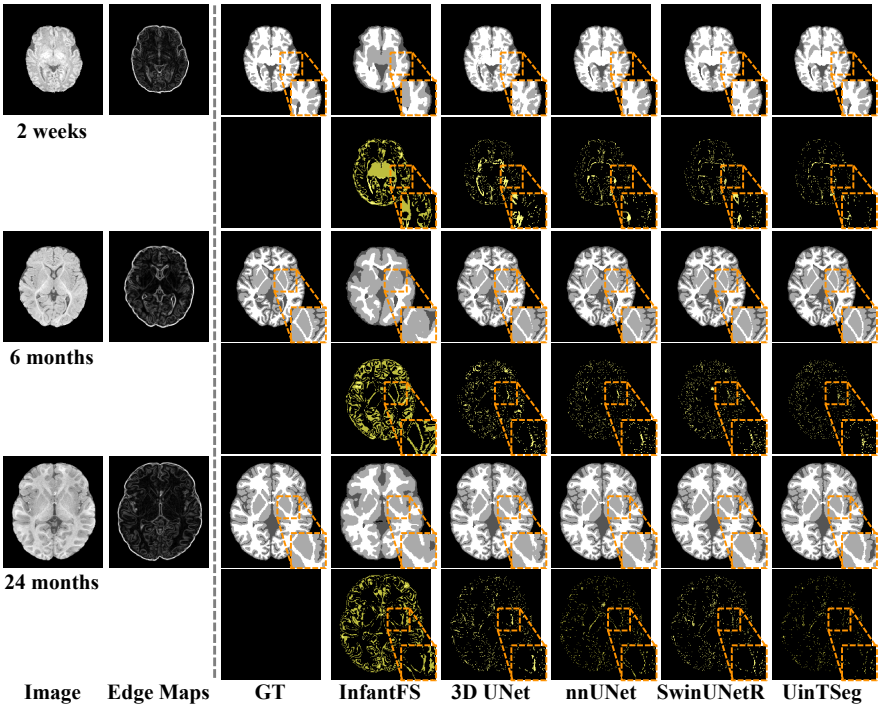

Fig. 3. Qualitative comparison of segmentation results using SOTA methods in three cases, including segmented images, corresponding close-up views, and error maps compared to GT. (yellow-colored voxels denote the segmentation errors)

Table 1 demonstrates quantitative evaluation for all the methods for infants aged 0-24 months. It is shown that our proposed framework obtains the highest *mean* Dice score, as well as the lowest HD and ASD, compared to the four SOTA methods. Besides, Table 2 also presents the evaluation results at the isointense phase. We can find that *UinTSeg* consistently shows superior performance over the five SOTA methods and even achieves better performance as the method TMSN [14], which is specifically tailored for the isointense phase.

To qualitatively evaluate our proposed framework, we carried out a visual comparison for three typical infant cases at three distinct ages, *i.e.*, 2 weeks, 6 months, and 24 months. As shown in Fig. 3, we can find that the predicted tissue maps obtained by our proposed *UinTSeg* (last column of the right panel) are close to the GT (first column of the right panel), especially in the subcortical regions, indicating that our proposed *UinTSeg* achieves the best visual perception among all the four SOTA methods, which is in line with quantitative evaluation. We can obtain the same conclusion also from the error maps (even rows in the middle panel) computed by absolute subtraction of the predicted tissue maps from GT ones. The performance improvement mainly arises from the intensity-

Table 3. Ablation study of our proposed each component in *UinTSeg*.

Method	Sobel Filtering	Boundary Extraction	Dice (%) ↑			HD (*mm*) ↓			ASD×10 (*mm*) ↓		
			CSF	GM	WM	CSF	GM	WM	CSF	GM	WM
SegNet			93.83±2.62	94.15±2.50	93.15±1.86	6.95±1.90	7.29±2.45	9.96±2.30	1.01±0.26	1.16±0.51	0.78±0.27
ASNet			94.61±2.24	94.59±2.17	94.55±1.43	7.14±2.06	7.13±2.53	9.61±2.22	0.91±0.23	7.13±2.52	0.62±0.20
ASNet	✓		95.11±2.25	95.39±1.97	94.98±1.65	7.09±2.28	6.76±2.48	9.12±2.13	0.79±0.23	0.92±0.40	0.56±0.28
UinTSeg	✓	✓	**95.84**±2.07	**95.98**±1.87	**95.70**±1.51	**6.57**±1.95	**6.96**±2.44	**8.88**±2.21	**0.68**±0.22	**0.80**±0.37	**0.48**±0.23

invariant anatomy guidance of the extracted tissue boundaries as well as the multi-scale tissue representations. The quantitative and qualitative evaluations consistently reveal the effectiveness of our proposed *UinTSeg*.

3.3 Ablation Studies

To validate the module effectiveness of *UinTSeg*, we conducted ablation studies (Table 3) by extending the baseline single-scale segmentation network SegNet with our proposed components, including the attention-based surrounding-aware segmentation Network (ASNet), Sobel filtering, and the boundary extraction network. As listed in Table 3, SegNet denotes the basic single-scale segmentation network using solely local patches; *ASNet* denotes the two branches segmentation network; *UinTSeg* denotes the complete segmentation framework that unifies *ASNet*, Sobel filtering, and boundary extraction.

Effectiveness of *ASNet*. As presented in Table 3, a notable improvement is observed when comparing *ASNet* (second row in Table 3) with the single-scale SegNet (first row in Table 3). It is shown that *ASNet* elevates the Dice score across three tissues from 93.71% to 94.58%, and consistent improvement can be found from HD and ASD, indicating that fused patch features with an enlarged receptive field bring necessary contextual information to guide segmentation in local.

Effectiveness of anatomy guidance. Compared to *ASNet* (second row), our proposed *UinTSeg* exploits *not only* the original T1w data, *but also* the *Sobel edge maps* and *extracted boundaries* of GM, WM, and CSF. As reported in the last rows of Table 3, we can find that incorporating *Sobel edge maps* as additional anatomy information into the input enhances Dice (third row of Table 3) by 0.58% compared to solely utilizing T1w data as input (second row of Table 3). Additionally, a notable improvement in segmenting GM, WM, and CSF tissues is observed across all the evaluated metrics by incorporating both intensity-invariant *Sobel edge maps* and *extracted boundaries* into the input (the last row of Table 3). In summary, our results highlight the effectiveness of integrating *intensity-invariant* anatomy information for guiding infant brain segmentation throughout this ongoing and dramatic development period.

4 Conclusion

In this study, we present a unified framework, *UinTSeg*, for brain tissue segmentation of infants aged from neonatal to 24 months based on T1w data. Unlike previous studies that are dedicated to training a range of isolated models for specific infant developmental periods, our framework enables precise tissue segmentation across the ongoing and dramatic development period using a single unified model. *UinTSeg* accommodates severe *variations in intensity* by leveraging *intensity-invariant* information of tissue boundaries. Extensive experiments have demonstrated that our proposed *UinTSeg* significantly outperforms five SOTA methods both quantitatively and qualitatively, particularly for the segmentation of isointense infant brain tissues. It underscores the effectiveness of integrating *intensity-invariant* anatomy information as well as contextual information in infant brain tissue segmentation, demonstrating potential in investigating early brain development and neurodevelopmental disorders.

Acknowledgments. This work was supported in part by National Natural Science Foundation of China (No. 62131015, 62250710165, 62203355, and U23A20295), the STI 2030-Major Projects (No. 2022ZD0209000), Shanghai Municipal Central Guided Local Science and Technology Development Fund (No. YDZX20233100001001), Science and Technology Commission of Shanghai Municipality (STCSM) (No. 21010502600), and The Key R&D Program of Guangdong Province, China (No. 2023B0303040001 and 2021B0101420006).

Disclosure of Interests. The authors have no competing interests to declare that are relevant to the content of this article.

References

1. Bui, T.D., Shin, J., Moon, T.: Skip-connected 3D denseNet for volumetric infant brain MRI segmentation. ***Biomedical Signal Processing and Control*** **54**, 101613 (2019)
2. Bui, T.D., Wang, L., Lin, W., Li, G., Shen, D.: 6-month infant brain MRI segmentation guided by 24-month data using cycle-consistent adversarial networks. In: IEEE 17th International Symposium on Biomedical Imaging (***ISBI***). pp. 359–362. IEEE (2020)
3. Dubois, J., Alison, M., Counsell, S.J., Hertz-Pannier, L., Hüppi, P.S., Benders, M.J.: MRI of the neonatal brain: A review of methodological challenges and neuroscientific advances. ***Journal of Magnetic Resonance Imaging*** **53**(5), 1318–1343 (2021)
4. He, K., Lian, C., Zhang, B., Zhang, X., Cao, X., Nie, D., Gao, Y., Zhang, J., Shen, D.: Hf-unet: Learning hierarchically inter-task relevance in multi-task u-net for accurate prostate segmentation in ct images. IEEE Transactions on Medical Imaging (***TMI***) **40**(8), 2118–2128 (2021)
5. He, Y., Nath, V., Yang, D., Tang, Y., Myronenko, A., Xu, D.: SwinUNETR-V2: Stronger swin transformers with stagewise convolutions for 3D medical image segmentation. In: International Conference on Medical Image Computing and Computer-Assisted Intervention (***MICCAI***). pp. 416–426. Springer (2023)

6. Herschkowitz, N.: Brain development in the fetus, neonate and infant. ***Neonatology*** **54**(1), 1–19 (1988)
7. Howell, B.R., Styner, M.A., Gao, W., Yap, P.T., Wang, L., Baluyot, K., Yacoub, E., Chen, G., Potts, T., Salzwedel, A., et al.: The UNC/UMN baby connectome project (BCP): An overview of the study design and protocol development. ***NeuroImage*** **185**, 891–905 (2019)
8. Ilyka, D., Johnson, M.H., Lloyd-Fox, S.: Infant social interactions and brain development: A systematic review. ***Neuroscience*** & ***Biobehavioral Reviews*** **130**, 448–469 (2021)
9. Isensee, F., Jaeger, P.F., Kohl, S.A., Petersen, J., Maier-Hein, K.H.: nnU-Net: A self-configuring method for deep learning-based biomedical image segmentation. ***Nature Methods*** **18**(2), 203–211 (2021)
10. Kanopoulos, N., Vasanthavada, N., Baker, R.L.: Design of an image edge detection filter using the Sobel operator. ***IEEE Journal of Solid-State Circuits*** **23**(2), 358–367 (1988)
11. Li, G., Wang, L., Shi, F., Gilmore, J.H., Lin, W., Shen, D.: Construction of 4d high-definition cortical surface atlases of infants: Methods and applications. Medical Image Analysis, (***MedIA***) **25**(1), 22–36 (2015)
12. Liu, F., Huang, J., Guo, L., Tang, H., Cai, X., Zhang, Y., Liu, J., Hua, R., Gu, J., Tao, T., Huang, Z., He, Y., Cao, Z., Wang, L., Wen, X., Chen, G., Wang, F., Lian, C., Shi, F., Wang, Q., Feng, J., Zhang, H., Shen, D.: Harmonizing multi-modality biases in infant development analysis with an integrated mri data processing pipeline. In: International Society for Magnetic Resonance in Medicine (***ISMRM***) (2024)
13. Liu, F., Wang, Y., Gu, J., Huang, J., Liu, J., Hua, R., Zhu, Y., Jiang, M., Shi, F., Zhang, H., Wang, Z., Feng, J., Wu, H., Shen, D.: Neoaudi tract: An automated tool for identifying auditory fiber bundles in infants. In: International Society for Magnetic Resonance in Medicine (***ISMRM***) (2024)
14. Liu, J., Liu, F., Sun, K., Liu, M., Sun, Y., Ge, Y., Shen, D.: Adult-like phase and multi-scale assistance for isointense infant brain tissue segmentation. In: International Conference on Medical Image Computing and Computer-Assisted Intervention (***MICCAI***). pp. 56–66. Springer (2023)
15. Ma, J., Chen, J., Ng, M., Huang, R., Li, Y., Li, C., Yang, X., Martel, A.L.: Loss odyssey in medical image segmentation. Medical Image Analysis, (***MedIA***) **71**, 102035 (2021)
16. Meltzoff, A.N., Kuhl, P.K., Movellan, J., Sejnowski, T.J.: Foundations for a new science of learning. ***Science*** **325**(5938), 284–288 (2009)
17. Nie, D., Wang, L., Gao, Y., Shen, D.: Fully convolutional networks for multi-modality isointense infant brain image segmentation. In: IEEE 13th International Symposium on Biomedical Imaging (***ISBI***). pp. 1342–1345. IEEE (2016)
18. Patro, S., Sahu, K.K.: Normalization: A preprocessing stage. arXiv preprint arXiv:1503.06462 (***arXiv***) (2015)
19. Ronneberger, O., Fischer, P., Brox, T.: U-Net: Convolutional networks for biomedical image segmentation. In: International Conference on Medical Image Computing and Computer-Assisted Intervention (***MICCAI***). pp. 234–241. Springer (2015)
20. Shi, F., Yap, P.T., Fan, Y., Gilmore, J.H., Lin, W., Shen, D.: Construction of multi-region-multi-reference atlases for neonatal brain MRI segmentation. ***NeuroImage*** **51**(2), 684–693 (2010)
21. Shi, F., Yap, P.T., Gao, W., Lin, W., Gilmore, J.H., Shen, D.: Altered structural connectivity in neonates at genetic risk for schizophrenia: A combined study using morphological and white matter networks. ***NeuroImage*** **62**(3), 1622–1633 (2012)

22. Sun, Y., Liu, J., Liu, F., Sun, K., Zhang, H., Shi, F., Feng, Q., Shen, D.: Consistent and accurate segmentation for serial infant brain mr images with registration assistance. In: International Workshop on Machine Learning in Medical Imaging, (***MLMI***). pp. 186–195. Springer (2023)
23. Taha, A.A., Hanbury, A.: Metrics for evaluating 3D medical image segmentation: Analysis, selection, and tool. ***BMC Medical Imaging*** **15**(1), 1–28 (2015)
24. Tierney, A.L., Nelson III, C.A.: Brain development and the role of experience in the early years. ***Zero to Three*** **30**(2), 9 (2009)
25. Wang, L., Shi, F., Gao, Y., Li, G., Gilmore, J.H., Lin, W., Shen, D.: Integration of sparse multi-modality representation and anatomical constraint for isointense infant brain MR image segmentation. ***NeuroImage*** **89**, 152–164 (2014)
26. Wang, L., Shi, F., Lin, W., Gilmore, J.H., Shen, D.: Automatic segmentation of neonatal images using convex optimization and coupled level sets. ***NeuroImage*** **58**(3), 805–817 (2011)
27. Wang, L., Wu, Z., Chen, L., Sun, Y., Lin, W., Li, G.: iBEAT V2. 0: A multisite-applicable, deep learning-based pipeline for infant cerebral cortical surface reconstruction. ***Nature Protocols*** **18**(5), 1488–1509 (2023)
28. Wang, M., Zhang, D., Huang, J., Yap, P.T., Shen, D., Liu, M.: Identifying autism spectrum disorder with multi-site fMRI via low-rank domain adaptation. IEEE Transactions on Medical Imaging (***TMI***) **39**(3), 644–655 (2019)
29. Zöllei, L., Iglesias, J.E., Ou, Y., Grant, P.E., Fischl, B.: Infant freesurfer: An automated segmentation and surface extraction pipeline for T1-weighted neuroimaging data of infants 0–2 years. ***NeuroImage*** **218**, 116946 (2020)